Article:
Wheeldon, Elizabeth, Dennis, Michael, Mao, Ningtao et al. (2025) Self-sorting multi-scale materials by self-assembling multi-component nanostructured gels in nonwoven fabrics. Chemical communications. pp. 10546-10549. ISSN: 1364-548X

https://doi.org/10.1039/D5CC02616D

ChemComm

COMMUNICATION

View Article Online
View Journal

Cite this: DOI: 10.1039/d5cc02616d

Received 8th May 2025,
Accepted 6th June 2025

DOI: 10.1039/d5cc02616d

rsc.li/chemcomm

Self-sorting multi-scale materials by self-assembling multi-component nanostructured gels in nonwoven fabrics†

Elizabeth Wheeldon,[a] Michael R. Dennis,[b] Ningtao Mao[c] and David K. Smith *[a]

Two supramolecular gelators self-sort, creating hybrid gels with small (*ca.* 15 nm) and large (*ca.* 500 nm) nanofibres that reinforce one another rheologically. When assembled in a nonwoven fabric, self-sorting yields a multi-scale material with fibres on multiple length-scales. The nanofibres control the air permeability of the fabric and the smaller nanofibres enhance the robustness of the larger nanofibre network under forcing airflow conditions.

Sample-spanning nanostructured networks can be created by self-assembly of low-molecular-weight gelators (LMWGs).[1] LMWGs assemble into anisotropic fibrils that typically bundle into fibres, which then interact with one another to form a sample-spanning network. Attention has increasingly focussed on multi-component systems combining different LMWGs.[2] Molecular-scale self-sorting can occur, in which different LMWGs assemble into their own nanostructures.[3] On the nanoscale, self-sorted nanostructures may form independent interpenetrated networks or interact preferentially with themselves or each other.[4] Understanding such processes is an important task.[5]

The use of nanofibres to create smart fabrics is of interest, for example in developing protective lightweight garments capable of active filtration, to remove pollutants or aerosolised toxic agents from the air, preventing skin contact.[6] Most nanofibers in fabrics are produced by electrospinning,[7] but supramolecular gel technology offers advantages, as fabrics can be loaded using the LMWG in solution, with self-assembly into nanofibres enhanced by drying, allowing for simple processing, suitable for textile industry workflows. In an early example, Raghavanpillai and co-workers assembled fluorinated amide- and urea-based organogelators on a nonwoven fabric,[8] yielding a composite with water/oil repellency. Sureshan and co-workers assembled a diyne-functionalised 4,6-*O*-benzylidene-β-D-galactopyranoside LMWG on cotton then photo-polymerised it to produce a semi-conducting fabric.[9] Schmidt and co-workers used hydrogen-bonded assemblies of benzene-1,3,5-tricarboxamide (BTA, Fig. 1), which form 100–500 nm fibres on nonwovens, for application in air filtration.[10] Changes in BTA structure and solvent influenced diameter, pore size distribution, and performance.[11] BTA was also applied to nonwovens *via* vapour deposition.[12] In 2021, Zhuang, Di and co-workers assembled 1,3:2,4-di(3,4-dimethylbenzylidene) sorbitol (DMDBS) nanofibres (10–30 nm) in nonwovens.[13]

Inspired by previous work, we wanted to assemble multiple LMWGs in fabrics. We reasoned that 1,3:2,4-dibenzylidenesorbitol[14] (DBS, Fig. 1) could assemble into fibres *ca.* 10–20 nm

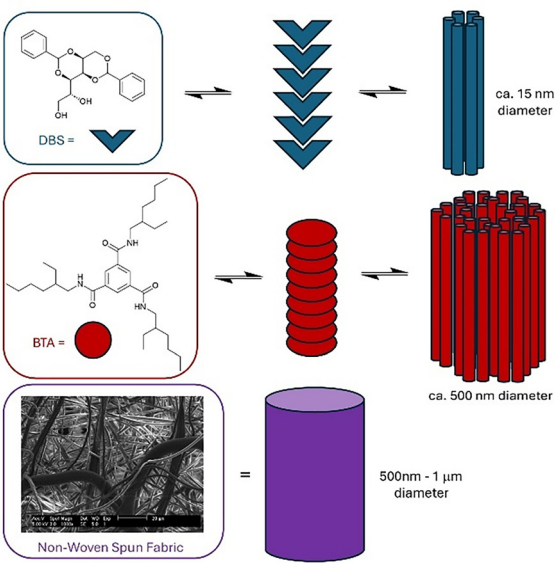

Fig. 1 Structures of DBS and BTA with schematics of assembly into fibrillar objects at different length scales. SEM image of nonwoven spun fabric and schematic highlighting microscale dimensions of fibres (scale bar: 20 μm).

[a] *Department of Chemistry, University of York, Heslington, York, YO10 5DD, UK. E-mail: david.smith@york.ac.uk*
[b] *Dstl Porton Down Salisbury, SP4 0JQ, UK*
[c] *School of Design, University of Leeds, Woodhouse Lane, Leeds, LS2 9JT, UK*

† Electronic supplementary information (ESI) available: Full experimental methods, additional data, collection of SEM images. See DOI: https://doi.org/10.1039/d5cc02616d

in diameter, BTA would form *ca.* 100–500 nm fibres, and a nonwoven meltblown polypropylene fabric would have microscale fibres (Fig. 1). The structural differences between DBS and BTA and their different assembly mechanisms led us to believe self-sorting was possible – we thus hoped to create 'multi-scale' materials.

Initially, we explored gels combining DBS and BTA. Previous work[10,11,15] led us to select methanol and 2-butanone as solvents to both support assembly and wet nonwoven fabrics. In the absence of fabric, DBS forms gels with a minimum gelation concentration (MGC) of 0.4% wt/vol in methanol and 0.6% wt/vol in 2-butanone. DBS is a solvent-tolerant LMWG, assembling through a variable combination of O–H···O hydrogen bonds and solvophobic/π−π interactions between aromatic rings.[16] In contrast, BTA only forms gels at elevated concentrations in methanol (>3.0% wt/vol) and although it formed gels in 2-butanone (MGC 0.6% wt/vol), they were very weak. BTA assembles primarily only *via* intermolecular amide hydrogen bonds, which is less effective/cooperative in H-bonding solvents like MeOH.[17]

Scanning electron microscopy (SEM) was performed on hot samples allowed to cool and dry on SEM stubs under ambient conditions (equivalent to fabric loading conditions – see below). DBS in methanol (0.6% wt/vol) gave flexible nanofibers *ca.* 15 nm in diameter (Fig. 2, top left). In contrast, BTA (0.6% wt/vol) in methanol formed rigid nanocrystalline objects with varying diameters (200–1000 nm), averaging *ca.* 700 nm (Fig. 2, top right). Although BTA forms supramolecular polymers, the rigid nanocrystalline fibres are less effective as sample-spanning gels than DBS nanofibres. On combining DBS and BTA (both 0.6% wt/vol) in methanol, the system self-sorted – large BTA nanofibres and much smaller DBS nanofibers were clearly observed (Fig. 2, bottom and Fig. S4, ESI†). The small DBS nanofibres were evenly distributed and coated the larger BTA nanofibres. DBS and BTA therefore appear to prefer narcissistic interactions.

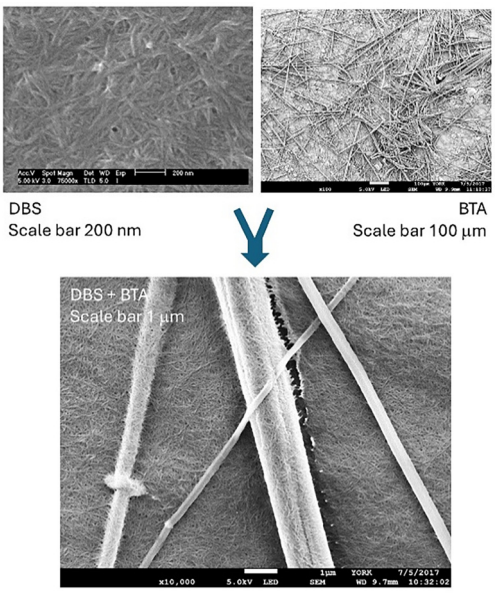

Fig. 2 SEM images of (top left) DBS gel (0.6% wt/vol) dried from methanol, scale bar = 200 nm (top right) BTA gel (0.6% wt/vol) dried from methanol, scale bar = 100 μm, and (bottom) DBS and BTA gel (0.6% wt/vol of each component) dried from methanol, scale bar = 1 μm.

Changing solvent to 2-butanone did not significantly change the DBS nanofibres but changed the nanoscale morphology of BTA, which formed more flexible, slightly smaller fibres (mean diameter *ca.* 450 nm), indicating less crystallinity. This was expected based on the prior work of Schmidt and co-workers,[10,11] and is consistent with the better gel-forming capacity of BTA in this less H-bonding solvent. SEM imaging of DBS and BTA (both 0.6% wt/vol) in 2-butanone indicated self-sorting of DBS–BTA into small/large nanofibres (Fig. S5, ESI†).

To better understand the gels, we performed rheology using a constant concentration of DBS (0.6% wt/vol) to maintain gel behaviour and adding increasing amounts of BTA (Fig. S1, ESI†). At low BTA loadings, gel stiffness was similar to DBS alone (G' = 1000–10 000 Pa). Once the BTA loading reached a threshold level, stiffness increased very significantly. In 2-butanone, stiffening occurred at 0.9% wt/vol BTA (G' = 53 600 Pa). This is roughly in-line with the MGC of BTA, but the increase in stiffness is far more than expected for the very soft BTA gels. This suggests a synergistic effect on mechanical performance when the networks combine, as sometimes observed for interpenetrating gel networks.[18] We propose that the BTA nanofibres reduce the effective distance that must be spanned by the DBS network (Fig. 2, bottom). Hence BTA nanofibres provide a scaffold that helps DBS form its sample-spanning network, stiffening the gel. In methanol, BTA-induced stiffening (G' = 28 300 Pa) occurred at 0.7% wt/vol. This is below the MGC, suggesting BTA assembly occurs, and although the BTA nanofibers cannot constitute an independent gel, they can act as a secondary network stiffening the DBS gel. BTA does not impact on DBS thermal stability (Table S1, ESI†), presumably the BTA fibres disassemble on heating.

^{1}H NMR spectroscopy further probed molecular-scale assembly (Fig. S2 and S3, ESI†). ^{1}H NMR spectra were recorded of both gelators individually at 0.6% wt/vol in CD_3OD with DMSO as an internal standard. LMWG that self-assembles into solid-like nanofibers cannot be detected, but mobile LMWG can be detected and quantified.[19] 52% of DBS was assembled, and 66% of BTA, further evidence that even below its MGC, BTA forms solid-like structures. When testing a mixture of DBS (0.6% wt/vol) and BTA (0.6% wt/vol), 67% of DBS and 66% of BTA were immobilised into nanofibres, similar to DBS and BTA individually, suggesting self-sorting.

These studies confirm DBS and BTA self-sort into their own networks, with very different nanoscale dimensions. The DBS network has more 'gel-like' properties, while the BTA network has greater crystallinity. These nanoscale assemblies collaborate at a network level to form hybrid gels with significantly enhanced stiffness.

We then studied assembly of DBS and BTA in a nonwoven polypropylene melt-blown fabric. Samples were prepared by dipping fabric into a hot (*ca.* 60 °C) solution of the LMWG for 5 min and leaving to cool and dry in ambient conditions. In

preliminary work, we monitored the mass of LMWG picked up by the fabric. A normalised 1.00 mg sample of nonwoven fabric had final masses of 1.17, 1.24, 1,40, 1.68 and 2.65 mg when using hot solutions of DBS in methanol with loadings of 0.4%, 1%, 2%, 5% and 10% respectively. This confirms DBS is taken up by the nonwoven fabric, and as concentration increases, the amount deposited increases. We then focussed on lower loadings of DBS and BTA (0.2–1.0% wt/vol), studying their pick-up in methanol and 2-butanone. A normalised 1.00 mg fabric sample had final masses of 1.10–1.25 mg, with greater mass increases at higher loadings. There were no systematic differences in uptake between DBS and BTA even though DBS has greater capacity for gel formation, nor were there significant solvent differences. This suggests LMWG is deposited by soaking and cooling/drying, rather than additional viscosity effects, as expected given fabric samples are prepared by dipping in low viscosity hot solutions.

SEM indicated that at 0.6% wt/vol loading, DBS and BTA retained their nanoscale morphologies when combined with the nonwoven fabric, with fabric-spanning networks being formed (Fig. 3, left). The very small (*ca.* 15 nm) DBS nanofibres are only easily visible at high magnification (Fig. S8, ESI†) – at lower magnification they appear as sheet-like objects spanning between nonwoven fibres. BTA forms much larger nanofibres, that appear interwoven with the even larger fibres of the nonwoven (Fig. S3, right, Fig. S10, S11, ESI†). The sheet-like membrane-type assemblies of small nanofibres observed for DBS are consistent with its more effective gelation.

The two LMWGs were then simultaneously combined with the nonwoven fabric using methanol as solvent. Three different fibre length scales were observed – fabric microfibres (*ca.* 1 μm), BTA nanofibres (*ca.* 700 nm) and DBS nanofibres (*ca.* 15 nm) (Fig. 4 and Fig. S14, ESI†). This is therefore a rare example of a system in which three different fibrillar structures are independently present, elegantly demonstrating how controlled self-assembly easily adds complexity to fabrics. The LMWGs provide uniform fabric coverage with minimal gaps between different fibres. The regularity of coverage and multiple different scales of fibres could be useful in terms of filtration.[6] This multi-component system was also tested with

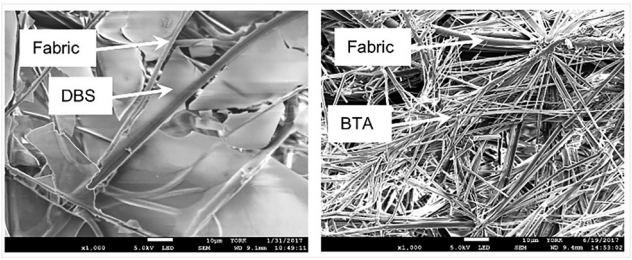

Fig. 3 SEM images of (left) DBS (0.6% wt/vol in methanol) dried onto nonwoven fabric forming sheet-like aggregates of small nanofibres that span between the nonwoven fabric fibres and (right) BTA (0.6% wt/vol in methanol) dried onto nonwoven fabric forming larger semi-rigid nanofibres that are interwoven with the nonwoven fabric fibres (scale bars = 10 μm).

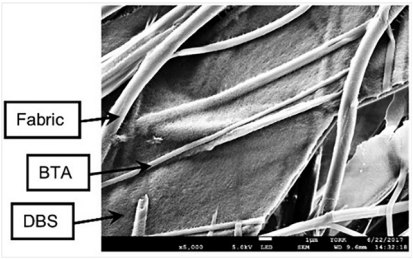

Fig. 4 SEM images of multi-scale material comprising DBS nanofibers, BTA nanofibers and nonwoven fabric microfibres, scale bar = 1 μm.

2-butanone as solvent (Fig. S15 and S16, ESI†). Again, three fibre sizes were distinguished, with BTA nanofibres being slightly smaller and more flexible than when dried from methanol. The fabric was not quite as well coated as with methanol, with some gaps observed (see below).

When modifying the nonwoven fabric as described above with a total LMWG loading of 1.2% wt/vol, its physical properties were significantly affected, becoming stiffer handle and losing some flexibility. For wearable applications, this would be undesirable, therefore lower LMWG concentrations were tested. Using a mixture of 0.3% wt/vol BTA and 0.3% wt/vol DBS on a nonwoven gave self-sorted DBS and BTA nanofibres (Fig. S17–S20, ESI†). In methanol, BTA formed larger, more rigid nanofibres that appeared to better support the aggregation of small DBS nanofibres leading to more uniform distribution, whereas in 2-butanone, the more flexible BTA nanofibres led to hybrid materials with pores. We also tested variable loadings of DBS and BTA, maintaining a total loading of 0.6% wt/vol (Fig. S21 and S22, ESI†). All systems exhibited self-sorting, even though solutions are well below their MGCs. Importantly, at this lower total loading, the physical properties of the fabric were not noticeably changed. We also made modified nonwovens with a total LMWG loading of 0.4% wt/vol (Fig. S23–S30, ESI†). In this case, DBS did not fully span the fabric. A total loading of 0.6% wt/vol was therefore optimal, combining effective coverage with desirable physical properties, and was scaled up for testing.

Air permeability testing was completed to British Standard EN ISO 9073-15:2008, which specifies a method of measuring the velocity of an air flow passing perpendicularly through 5 cm^2 of test fabric under an air pressure differential of 100 Pa over a given time period. Control fabrics that had been soaked in pure methanol or 2-butanone had permeabilities of 47 and 41 $cm^3\ cm^{-2}\ s^{-1}$ respectively. For fabrics loaded with either DBS or BTA, air permeability fell as loading increased until there was almost no air permeability ($<2\ cm^3\ cm^{-2}\ s^{-1}$) at 2.0% wt/vol (Fig. S34, ESI†), indicating DBS/BTA nanofibre networks limit air permeability by physically blocking nonwoven fabric pores.

We selected 0.6% wt/vol for further study, as it had intermediate air permeability and desirable characteristics described above. All fabrics treated with DBS/BTA in different ratios at a total loading of 0.6% wt/vol had reduced air permeabilities (5–30 $cm^3\ cm^2\ s^{-1}$, Fig. S35, ESI†). The samples made

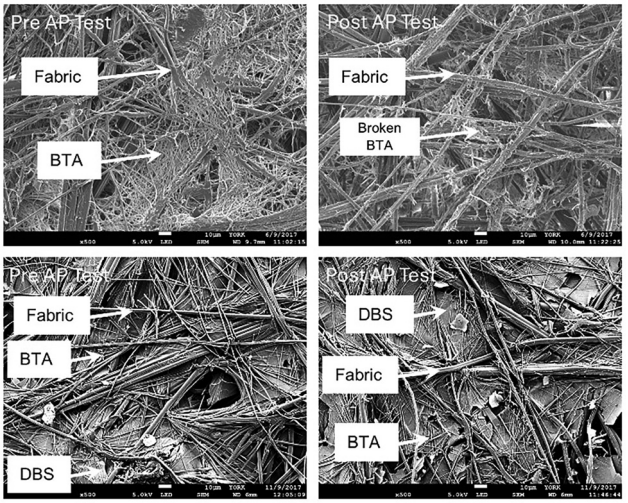

Fig. 5 SEM images taken before (left) and after (right) air permeability testing. (Top) Images of nonwoven fabric loaded with BTA (1.0% wt/vol) in 2-butanone. (Bottom) Images of nonwoven fabric loaded with BTA (0.3% wt/vol) and DBS (0.3% wt/vol) in methanol. All scale bars = 10 μm.

in methanol (5–20 cm^3 cm^2 s^{-1}) had lower air permeability than using 2-butanone (10–30 cm^3 cm^2 s^{-1}), with the solvent-induced difference being beyond error range. This is consistent with more effective fabric coverage in methanol as observed by SEM. The DBS : BTA ratio did not have significant effect on air permeability. We also tested DBS/BTA at a total loading of 0.4% wt/vol – again the LMWG networks lowered air permeability (Fig. S36, ESI†), but it was slightly higher than at 0.6% wt/vol, particularly in 2-butanone (20–30 cm^3 cm^{-2} s^{-1}) which had less effective fabric spanning (see above).

Air permeability testing is a forcing technique – there is potential for damage. We thus performed SEM imaging on fabric samples after testing. For DBS alone, the very small diameter DBS nanofibre network remained intact (Fig. S31–S33). However, BTA had evidence of damage to the self-assembled nanofibers, with broken pieces observed on the nonwoven (Fig. 5, top). We reason that forcing conditions break the more disperse, weaker network of larger BTA nanofibres. For the two-component system, both DBS and BTA networks appeared intact after testing (Fig. 5, bottom), even at low loading (0.4% wt/vol). This suggests DBS and BTA networks reinforce each other, as found in gel rheology. The multi-component system therefore retains the benefit of both DBS and BTA nanofibre networks but has greater robustness than BTA alone.

In summary, LMWGs based on DBS and BTA self-sort, with DBS forming small nanofibers (*ca.* 15 nm), while BTA forms much larger nanofibers (*ca.* 500 nm), with the precise diameter depending on solvent. Rheology indicates orthogonal self-assembled networks form below the MGC, and that assembled BTA nanofibres significantly enhance the stiffness of a DBS gel. The self-sorting methodology enables easy fabrication of interpenetrated multi-scale fibrillar materials by self-assembling the LMWGs in a nonwoven fabric *via* a simple mixing and dipping protocol. The self-assembled gel nanofibers lower the air permeability of the fabric with more extensive assembled networks (controlled by loading level or solvent) having a greater effect. SEM analysis after permeability testing suggests the self-sorted dual network is less susceptible to damage than a BTA-only network. The easy fabrication of multiscale fibrillar materials, combined with their enhanced robustness suggests potential advantages of this self-sorting approach in air filtration and/or the creation of next-generation wearable technologies.

This work was supported by DSTL *via* a PhD studentship to EAW.

Data availability

All data are provided in the ESI.†

Conflicts of interest

There are no conflicts to declare.

Notes and references

1 D. K. Smith, *Soft Matter*, 2024, **20**, 10–70.
2 (*a*) A. R. Hirst and D. K. Smith, *Chem. – Eur. J.*, 2005, **11**, 5496–5508; (*b*) L. E. Buerkle and S. J. Rowan, *Chem. Soc. Rev.*, 2012, **41**, 6089–6102.
3 (*a*) K. Sugiyasu, *et al.*, *Chem. Mater.*, 2008, **20**, 2863–2865; (*b*) J. R. Moffat and D. K. Smith, *Chem. Commun.*, 2009, 316–318; (*c*) S. Onogi, *et al.*, *Nat. Chem.*, 2016, **8**, 743–752.
4 (*a*) R. Kubota, *et al.*, *Nat. Commun.*, 2020, **11**, 4100; (*b*) K. Nakamura, *et al.*, *Nat. Commun.*, 2023, **14**, 1696.
5 (*a*) E. R. Draper and D. J. Adams, *Chem. Soc. Rev.*, 2018, **47**, 3395–3405; (*b*) D. J. Adams, *J. Am. Chem. Soc.*, 2022, **144**, 11047–11053.
6 (*a*) L. Maduna and A. Patnaik, *Text. Prog.*, 2017, **49**, 173–247; (*b*) A. Nadi, *et al.*, *Text. Prog.*, 2018, **50**, 67–108.
7 J. Xue, *et al.*, *Chem. Rev.*, 2019, **119**, 5298–5415.
8 (*a*) A. Raghavanpillai, S. Reinartz and K. W. Hutchenson, *J. Fluorine Chem.*, 2009, **130**, 410–417; (*b*) A. Raghavanpillai, V. A. Franco and W. E. Meredith, *J. Fluorine Chem.*, 2012, **135**, 187–194.
9 B. P. Krishnan, *et al.*, *Angew. Chem., Int. Ed.*, 2016, **55**, 2345–2349.
10 H. Misslitz, K. Kreger and H.-W. Schmidt, *Small*, 2013, **9**, 2053–2058.
11 (*a*) D. Weiss, *et al.*, *ACS Appl. Mater. Interfaces*, 2016, **8**, 14885–14892; (*b*) M. Burgard, *et al.*, *Adv. Funct. Mater.*, 2019, **29**, 1903166; (*c*) M. Drummer, *et al.*, *ACS Appl. Mater. Interfaces*, 2021, **13**, 34818–34828; (*d*) A. Frank, *et al.*, *Macromol. Rapid Commun.*, 2022, **43**, 2200052.
12 (*a*) D. Schröder, *et al.*, *Adv. Mater. Interfaces*, 2024, **11**, 2400259; (*b*) D. Schröder, *et al.*, *ACS Appl. Mater. Interfaces*, 2025, **17**, 14569–14577.
13 M. Hu, *et al.*, *J. Mater. Chem. A*, 2021, **9**, 14093–14100.
14 B. O. Okesola, *et al.*, *Soft Matter*, 2015, **11**, 4768–4787.
15 E. Wheeldon, PhD thesis, University of York, 2018.
16 (*a*) E. A. Wilder, R. J. Spontak and C. K. Hall, *Mol. Phys.*, 2003, **101**, 3017–3027; (*b*) J. Li, *et al.*, *Langmuir*, 2014, **30**, 13422–13429.
17 C. Kulkami, E. W. Meijer and A. R. A. Palmans, *Acc. Chem. Res.*, 2017, **50**, 1928–1936.
18 E. S. Dragan, *Chem. Eng. J.*, 2014, **243**, 572–590.
19 B. Escuder, M. Llusar and J. F. Miravet, *J. Org. Chem.*, 2006, **71**, 7747–7752.

